J Solid State Electrochem (1999) 3: 187–192

ORIGINAL PAPER

Francisco Prieto · Emma Hill · Barry A. Coles
Richard G. Compton · John H. Atherton

Application of the high-speed channel flow cell to reactive chemistry at solid surfaces

Received: 1 September 1998 / Accepted: 2 November 1998

Abstract A high-speed channel flow cell is used to study the reaction of solid *p*-chloranil with basic aqueous solutions. Dissolution of the solid is shown to be induced by reaction of OH^- ions at the solid/liquid interface and appropriate kinetic parameters are reported.

Key words *p*-Chloranil · Channel flow cell · Solid/liquid interface

Introduction

The fundamental study of reactions between solid and liquid phase species is the subject of rapidly growing attention [1, 2], not least because of their widespread synthetic, environmental and industrial importance. Diverse techniques are emerging for kinetic and mechanistic studies, including hydrodynamic methods, scanning electrochemical microscopy (SECM) and atomic force microscopy (AFM). The application of these different methods has been recently reviewed [2]. SECM can provide spatially resolved kinetic information whilst the AFM approach is to image reacting, or dissolving, surfaces under liquid [3–9]. By monitoring the evolution of surface structural features in real time, such as the translation of steps across the surface [3, 4, 6] or the growth of nuclei [9], the rate of reaction/dissolution may be inferred and estimates of the corresponding rate constants made. Alternatively, the absolute height of the surface may be measured and used to give surface averaged rates [8, 9]. The latter approach is particularly powerful when used in conjunction with a controlled and known flow [10, 11]. Alternatively, a purely kinetic approach is to employ a channel flow cell (CFC) [12–14]. This comprises a rectangular duct through which the solution of interest flows under laminar conditions. The solid reactant, in the form of a single crystal or a pellet of compacted powder, is embedded smoothly in one wall of the flow cell (Fig. 1) and a suitable detector, often an amperometric electrode, is located immediately downstream of the solid to monitor either the release of products or the consumption of reactants. Since the flow is laminar and, for appropriately designed cells, takes the form of the well-characterised parabolic Poiseuille flow, the mass transport between the detector and the reactive interface is calculable, so permitting quantitative inferences about the interfacial chemistry from fluxes or concentrations measured at the detector. In particular, the measurement of the detector signal as a function of flow rate provides a sensitive and discriminating method for characterising the mechanism of the interfacial reaction for the deduction of the corresponding rate constant(s) [12–14].

In this paper we report the design and application of a CFC for the study of reactions at solid/liquid interfaces which enjoys substantially higher rates of mass transport than hitherto available in such devices. Specifically, building on our experience in developing a high-speed channel cell for electrochemical measurements [15–17], we locate a microband electrode downstream of, and immediate adjacent to, the solid surface of interest. Using a pressurised system, this allowed volume flow rates in excess of 1 cm^3 s^{-1} through a channel cell no more than 100 μm in depth. The device is applied to the study of the dissolution of *p*-chloranil as induced by the reaction of hydroxide ions with the organic solid [18].

F. Prieto · E. Hill · B.A. Coles · R.G. Compton (✉)
Physical and Theoretical Chemistry Laboratory,
Oxford University, South Parks Road, Oxford OX1 3QZ, UK

J.H. Atherton
Zeneca Huddersfield Works, P.O. Box A38, Leeds Road,
Huddersfield HD2 1FF, UK

Experimental

The fast flow system has been described previously [15]. In essence, a pressurised system is used to force solutions through the channel

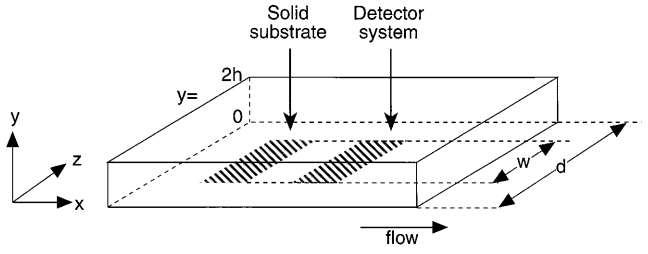

Fig. 1 Schematic diagram of a channel flow cell as used in this work

cell, fabricated in silica (Optiglass, Hainault, Essex, UK) and shown schematically in Fig. 2. The cross-sectional area of the flow cell is 2 mm × 0.1 mm. The cell was closed with a cover plate, shown schematically in Fig. 3, in the form of a pyrex block with a 3 mm diameter hole through the centre to accommodate the working electrode and crystal combination. The latter was fabricated by mating a length of platinum foil, 1 mm × 5 mm × 25 μm, back-to-back with the single crystal of *p*-chloranil with a thin layer of adhesive (cyanoacrylate adhesive, RS Components, Corby, UK). The latter also prevented any Faradaic current at the foil resulting from any redox reaction at the three-phase Pt/chloranil/electrolyte boundary. The width of the platinum foil was purposely chosen to be narrower in width than the crystal, ensuring minimal edge effects on the electrode. The 5 mm length acted as the electrical contact, the 1 mm dimension being the width of the electrode and the 25 μm dimension being the length. The crystal/electrode assembly was located in the correct orientation using a small amount of Blutak

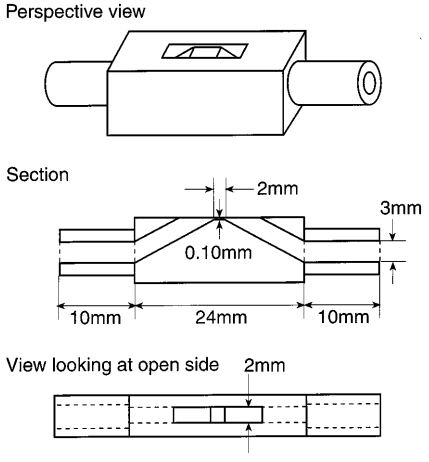

Fig. 2 High-speed channel flow cell showing a perspective view and the principal dimensions

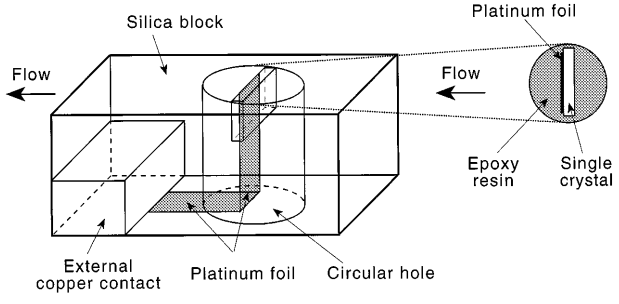

Fig. 3 Schematic diagram showing the cover plate containing a platinum microband electrode and the crystal of *p*-chloranil

(Bostik, Leicester, UK). Particular care was taken to mount the electrode/crystal component slightly proud of the cover plate surface with the electrode width as close to perpendicular as possible to the length of the cover plate and therefore the direction of flow. The crystal/electrode assembly was then fixed into position by pouring an excess of epoxy resin (Casting Araldite, Ciba Geigy, Cambridge, UK) from the top face. Placed inside a desiccator, the assembly was put under vacuum several times, in order to remove any gas from the resin prior to setting. The final preparation of the cover plate was to grind the crystal/electrode assembly down to flush with the Pyrex block. This was achieved using progressively finer grades of silicon carbide paper (Acton and Borman, Stevenage, UK) down to 1000 grade. The final polish involved a 0.3 micron grade aqueous alumina slurry supported on a soft pad (PSU-S, Kemet International, Kent, UK). The electrical contact for the working electrode was achieved by soldering the "tail" of the platinum foil to a copper strip, bonded to the back of the cover plate with epoxy resin (Araldite, Evode, Stafford, UK), which also served to protect the soldered joint. The precise dimensions of the working electrode and crystal were determined using a travelling microscope. Typical dimensions were such that the length of the crystal in the direction of flow was 0.5–1 mm.

Voltammetry was conducted using a conventional three-electrode potentiostat with a platinum coil counter electrode located downstream of the crystal/microband electrode combination and an upstream platinum wire pseudo-reference electrode.

Commercially available *p*-chloranil (Aldrich, 99%) was employed without further purification. Crystals of *p*-chloranil were grown from saturated solutions of *p*-chloranil in toluene, seeded with smaller pre-selected crystals by slow cooling of the saturated solution from 55 °C to room temperature over a period of 168 h in a 500 ml crystal growing flask. The solution was kept in motion by a slowly rotating paddle to ensure solution homogeneity. The solution cooling rate was controlled by using a home-built programmable temperature water bath described previously [18]. The crystals used for CFC experiments were approximately 0.05 × 0.2 × 0.2 cm in size with the 0.2 × 0.2 face corresponding to the 010 cleavage plane of *p*-chloranil. The latter face was cut to ca. 0.05 × 0.2 cm when incorporated into the flow cell. Suitably sized crystals prepared in this way were characterised using X-ray diffraction techniques. The unit cell dimensions and the unit cell volume were in excellent agreement with literature [19]. Experiments were conducted on the 010 and 100 faces. The identity of the latter was inferred by comparison with dissolution data obtained from large crystals of *p*-chloranil in a conventional CFC [20].

Potassium chloride (>99%) and volumetric standard grade potassium hydroxide (both Aldrich) were used without further purification. Experiments were conducted using solutions containing 0.2 M KCl with a range of KOH concentrations (15×10^{-3} M, 30×10^{-3} M, 50×10^{-3} M, 100×10^{-3} M and 200×10^{-3} M) spanning an approximate pH range of 12.2–13.3. A precise measure of solution pH was made using a pre-calibrated glass combination electrode (ABS) and meter (Model 7020, Electronic Instruments). All solutions were purged with argon (B.O.C 99.99%) prior to use.

Supporting numerical theory was generated from programs written in FORTRAN 77 and executed on a Silicon Graphics Origin 2000. Data analysis was performed using software written in Borland Turbo C and executed on an IBM-PC, with a 486 chip, running under MS DOS.

Results and discussion

Experiments were conducted using the platinum microband electrode to monitor species released from the 010 and 100 faces of *p*-chloranil crystals exposed to flowing aqueous solutions of 0.2 M KCl containing variable amounts of KOH in the range 15–200 mM. For all experiments a single voltammetric wave was seen with a

flow rate dependent halfwave potential of between −0.41 and −0.33 V (vs. Pt pseudo-reference electrode), with the former value corresponding to the limit of negligible flow rate. Typical voltammetry is shown in Fig. 4. The magnitude of the transport limited current decreased as a function of increasing volume flow rate for a given value of the solution pH. The species responsible for the voltammetric wave may be assigned to a short-lived, hydroxy adduct of *p*-chloranil and shows a closely similar half-wave potential to that seen for such a molecule in analogous experiments conducted using a conventional CFC [18]. On the basis of conventional CFC measurements and other data, including stopped flow and spectroscopic experiments, the general reaction scheme given in Fig. 5 has been deduced and modelled kinetically on the basis of the simplified scheme in Fig. 6 [18]. In the latter the labels A, B and C relate to voltammetrically discernible species; A is seen both in conventional CFC experiments and the fast flow results reported here, whilst B and C are only visible under conditions of slower mass transport [18] because of the finite time required for the decomposition of A. In the fast flow experiment, species B and C are only formed downstream of the microband electrode detector and hence do not appear in the voltammetry (Fig. 4). Typical transport limited current data for the reduction of A as a function of the mass transport rate are shown in Fig. 7 for various concentrations of hydroxide.

Data such as that shown in Fig. 7 were modelled to see if it was consistent with various possible dissolution models. In all cases the homogeneous chemistry summarised in Fig. 6 was incorporated to permit the inference of the detector signal (due to A) with solution flow rate. The steady-state convective diffusion equations which describe the distribution of the mechanistically significant species within the flow cell are as follows.

Species A:

$$0 = D_{\mathrm{A}}\frac{\partial^2[\mathrm{A}]}{\partial y^2} - v_x\frac{\partial[\mathrm{A}]}{\partial x} - k_1[\mathrm{A}][\mathrm{OH}^-]$$

Species B:

$$0 = D_{\mathrm{B}}\frac{\partial^2[\mathrm{B}]}{\partial y^2} - v_x\frac{\partial[\mathrm{B}]}{\partial x} + k_1[\mathrm{A}][\mathrm{OH}^-] - k_{2\mathrm{f}}[\mathrm{B}][\mathrm{OH}^-] + k_{2\mathrm{b}}[\mathrm{C}]$$

Species C:

$$0 = D_{\mathrm{C}}\frac{\partial^2[\mathrm{C}]}{\partial y^2} - v_x\frac{\partial[\mathrm{C}]}{\partial x} - k_3[\mathrm{C}] + k_{2\mathrm{f}}[\mathrm{B}][\mathrm{OH}^-] - k_{2\mathrm{b}}[\mathrm{C}]$$

Species OH^-

$$0 = D_{\mathrm{OH}^-}\frac{\partial^2[\mathrm{OH}^-]}{\partial y^2} - v_x\frac{\partial[\mathrm{OH}^-]}{\partial x} - k_1[\mathrm{A}][\mathrm{OH}^-] - k_{2\mathrm{f}}[\mathrm{B}][\mathrm{OH}^-] + k_{2\mathrm{b}}[\mathrm{C}]$$

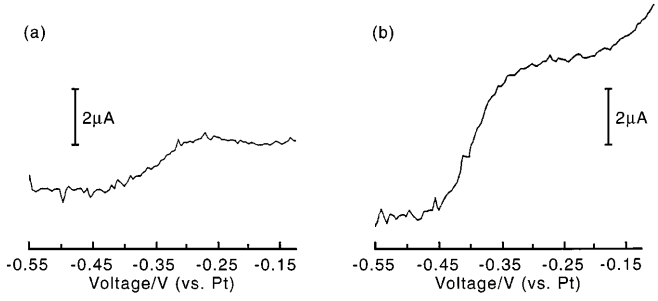

Fig. 4 Typical voltammograms measured downstream of a dissolving 100 face of *p*-chloranil at flow rates of **a** 1.7 $cm^3\ s^{-1}$ and **b** 0.02 $cm^3\ s^{-1}$

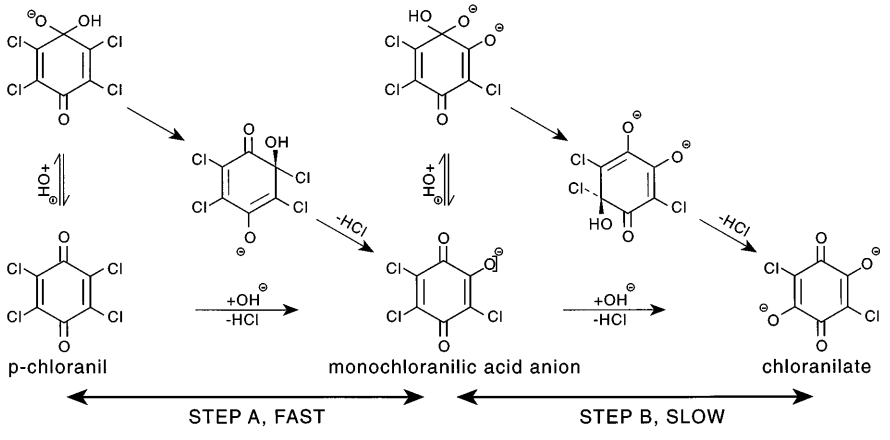

Fig. 5 General mechanistic scheme for the reactive dissolution of *p*-chloranil

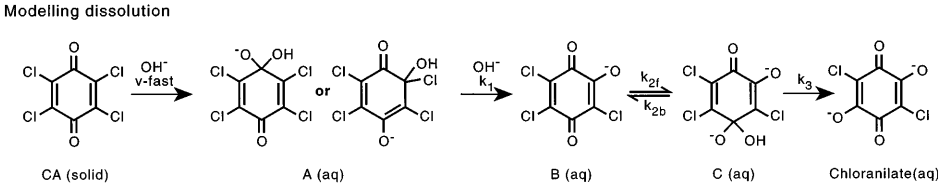

Fig. 6 Simplified scheme for the *p*-chloranil dissolution used for kinetic modelling [18]

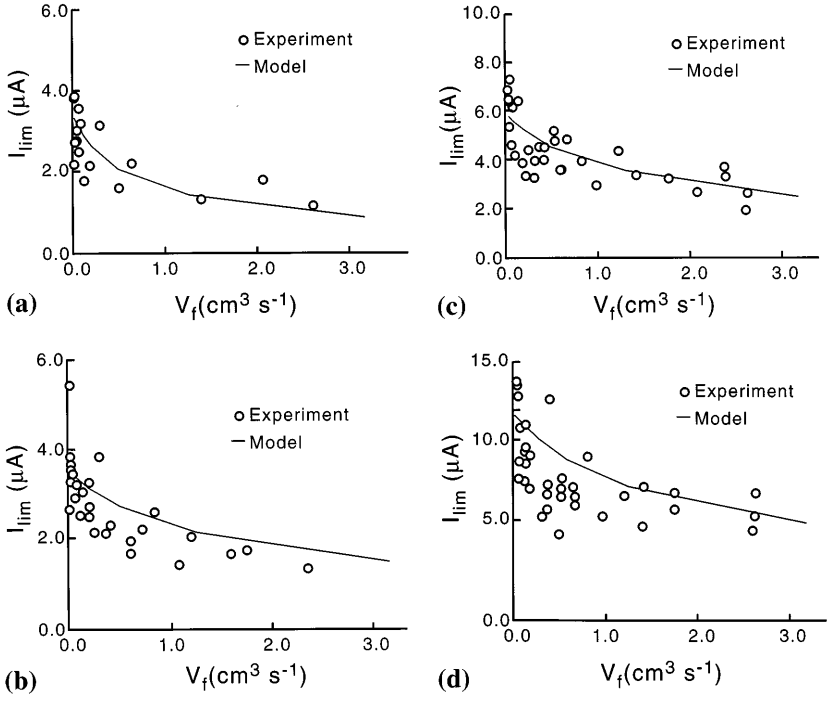

Fig. 7 Experimentally measured transport limited currents as a function of flow rate for the dissolution of the 100 face of *p*-chloranil in **a** 15 mM, **b** 30 mM and **c** 50 mM KOH/0.2 M KCl solution. The *solid line* shows the theoretical behaviour calculated using the heterogeneous dissolution model (see text)

where the coordinates x and y are defined in Fig. 1. Note that it is known that $k_1 = 1.25 \times 10^5$ mol^{-1} cm^3 s^{-1}, $k_{2f}/k_{2b} = 200$ M, k_3 has a value near 5×10^{-4} s^{-1}, $D_{OH^-} = 5.3 \times 10^{-5}$ cm^2 s^{-1}, and D_A, D_B and D_C can be estimated (to within 10%) using the established Wilke Chang correlation [21]. In all modelling it was assumed that B and C were in equilibrium so that k_{2f} and k_{2b} were made very large (10^7 mol^{-1} cm^3 s^{-1} and 50 s^{-1}, respectively) relative to the rates of transport in the cell [18].

The transport equations together with the above data permit the inference of the detector electrode current, provided boundary conditions are specified to describe the chemistry at the *p*-chloranil/solution interface, as discussed below. The convective-diffusion problem is then readily solved using the Backwards Implicit Finite Difference Method applied as described elsewhere [18, 22]. No new issues were encountered in this application and the reader is directed to the literature for appropriate details. The computations, when made for a known cell geometry, predict the concentrations of species A, B, C and OH^- throughout the flow cell as functions of flow rate for assumed values of the parameter(s) describing the appropriate interfacial boundary condition (vide infra). The latter are the only adjustable parameters in the model. The resulting concentration profiles are used to predict the current at the detector electrode. For this, further boundary conditions need to be incorporated into the computations relating to the detector electrode surface where a zero concentration of A, B and C is specified together with a zero flux of OH^- (flux $\approx D_{OH^-}\partial[OH^-]/\partial y$).

First, the modelling confirmed that negligible concentrations of B and C are generated in the vicinity of the microband detector electrode, so confirming the voltammetric non-observation of species B and C (vide supra). This observation permitted simplified convective diffusion equations to be used in subsequent modelling as described below.

Second, in the manner described above, the dependence of the detector signal due to the reduction of A on flow rate can be identified and the theoretical data can be related to the experimental results. Best fit values of the interfacial parameters were obtained by minimising the deviation between the theoretical and experimental currents in a least squares sense. Three separate possible models were considered for the interfacial chemistry. The first supposed a saturated concentration of *p*-chloranil (P) at the dissolving solid:

$$P(s) \rightleftharpoons P(aq)$$

$$P(aq) + OH^-(aq) \xrightarrow{k'} A(aq)$$

The interface can be assumed to be saturated with either P or A. The second model is similar to the first except that it assumes a constant flux for the dissolution rate of P:

$$P(s) \xrightarrow{k_d} P(aq)$$

$$P(aq) + OH^-(aq) \xrightarrow{k'} A(aq)$$

where k_d (mol cm^{-2} s^{-1}) describes the rate of dissolution:

$$D_P\left(\frac{\partial[P]}{\partial y}\right)_{y=0} = -k_{het}$$

Last, the dissolution is assumed to occur via heterogeneous reaction of OH^- at the solid surface:

$$P(s) + OH^-(aq) \xrightarrow{k_{het}} A(aq)$$

The rate constant k_{het} (cm s^{-1}) describes the release of the species A:

$$D_A \left(\frac{\partial [A]}{\partial y} \right)_{y=0} = -k_{het} [OH^-]_{y=0}$$

In addition, it is useful to further consider the possibility of distinguishing between different possible hydroxy adducts A_1 and A_2 as defined in Fig. 8. This requires the following additional step to be considered

$$A_1(aq) \xrightarrow{k''} A_2(aq)$$

In this case, species A in the above is then understood to represent the adduct A_1; alternatively, if the isomerisation of A_1 into A_2 is omitted from the modelling, then the assignment of the molecular structures A_1 or A_2 to the species A is kinetically insignificant [18]. Either or both A_1 and A_2 may be considered to be voltammetrically active.

Comparison of the experimental data with modelling based on the above three kinetic schemes showed that the first two outlined above, in which there is free chloranil present in solution, did not fit unless physically unrealistic values of k' were adopted which were a factor of 10^3 slower than the value (1.8×10^7 mol^{-1} dm^3 s^{-1}) measured experimentally in homogeneous solution using stopped flow experiments [23]. Further, if k' was treated as an adjustable parameter value the first two models were additionally unsatisfactory in that the saturated surface model predicted concentrations well below the known aqueous solubility of *p*-chloranil [24], whilst in the case of a constant flux of *p*-chloranil release a systematic change of k_d with pH was required to fit the data across the full range of hydroxide concentrations studied.

The model of hydroxide induced dissolution followed by isomerisation of voltammetrically inactive A_1 into active A_2 was found to be the only model that fitted all experimental data over the full range of flow rates and pH values used. Typical fits are given in Fig. 7 and the associated best fit kinetic parameters were $k_{het} = 1.5 \pm 0.5 \times 10^{-4}$ cm s^{-1} (010 face [25]) or $5.0 \pm 0.5 \times 10^{-4}$ cm s^{-1} (100 face[1]) and $k'' = 1.25 \times 10^3$ s^{-1}. The first value for k_{het} is in good agreement with that inferred from conventional CFC experiments. The latter are, however, "blind" to the occurrence of the A_1 to A_2 isomerisation step, which occurs on the millisecond timescale and it can be appreciated that the use of the fast flow channel permits the deduction that the hydroxide induced dissolution of *p*-chloranil leads first to the hydroxy adduct, A_1 (Fig. 8), which then rapidly converts to A_2.

[1]Note that the designations 010 and 100 refer to the faces of the organic crystal as exposed in the flow cell. As detailed in the experimental section the surfaces are lapped and polished extensively before study so that the kinetic parameters reported refer to the faces so treated and not to perfect single crystal faces.

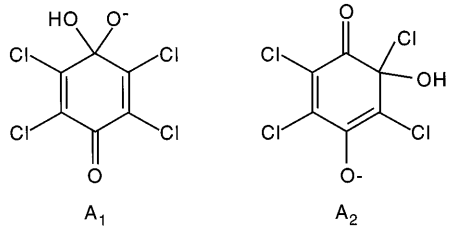

Fig. 8 The two possible hydroxy adducts of *p*-chloranil: A_1 and A_2

Conclusions

The dissolution of *p*-chloranil in aqueous base proceeds via the reaction of OH^- ions at the solid/liquid interface with the formation of the intermediate hydroxy adduct A_1:

$$P(s) + OH^-(aq) \xrightarrow{k_{het}} A(aq)$$

followed by the rapid isomerisation of the latter which occurs on the millisecond timescale:

$$A_1(aq) \xrightarrow{k''} A_2(aq)$$

The use of a high-speed channel flow cell thus allows the observation of processes too fast to be seen in a conventional CFC and, in particular, to confirm (or not) mechanistic conclusions drawn from the latter using a much wider range of mass transport conditions.

Acknowledgements We thank EPSRC and Zeneca plc for a studentship for E.H. and the EU for financial support for F.P. (Grant No. ERBFMBICT950219).

References

1. Atherton JH (1994) Res Chem Kinet 2: 193
2. Macpherson JV, Unwin PR (1995) Prog React Kinet 20: 185
3. Hillner PE, Manne S, Gratz AJ (1992) Ultramicroscopy 42–44: 1387
4. Hillner PE, Manne S, Gratz AJ (1992) Geology 20: 359
5. Shakesheff KM, Davies MC, Domb A, Jackson DE, Roberts CJ, Tendler SJB, Williams PM (1995) Macromolecules 28: 1108
6. Hall C, Cullen DC (1996) AIChEJ 42: 232
7. Sanders GHW, Booth J, Compton RG (1997) Langmuir 13: 3080
8. Hong Q, Suárez MF, Coles BA, Compton RG (1997) J Phys Chem 101: 5557
9. Booth J, Compton RG, Atherton JH (1998) J Phys Chem B 102: 3980
10. Coles BA, Compton RG, Booth J, Hong Q, Sanders GHW (1997) J Chem Soc Chem Commun 1473
11. Coles BA, Compton RG, Suárez M, Booth J, Hong Q, Sanders GHW (1998) Langmuir 14: 218
12. Compton RG, Harding MS, Pluck MR, Atherton JH, Brennan CM (1993) J Phys Chem 97: 10461

13. Compton RG, Harding MS, Atherton JH, Brennan CM (1993) J Phys Chem 97: 4677
14. Tam KY, Compton RG, Atherton JH, Brennan CM, Docherty R (1996) J Am Chem Soc 118: 4419
15. Rees NV, Dryfe RAW, Cooper JA, Coles BA, Compton RG, Davies SG, McCarthy TD (1995) J Phys Chem 99: 7096
16. Rees NV, Alden JA, Dryfe RAW, Coles BA, Compton RG (1995) J Phys Chem 99: 14813
16. Prieto F, Aixill WJ, Alden JA, Dryfe RAW, Coles BA, Compton RG (1995) J Phys Chem 101: 5540
17. Coles BA, Dryfe RAW, Rees NV, Compton RG, Davies SG, McCarthy TD (1996) J Electroanal Chem 411: 121
18. Booth J, Sanders GHW, Compton RG, Atherton JH, Brennan CM (1997) J Electroanal Chem 440: 83
19. van Weperen KJ, Visser GJ (1972) Acta Crystallogr B28: 338
20. Hill E, Lloyd-Williams RR, Compton RG, Atherton JH (1999) J Solid State Electrochem (in press)
21. Wilke CR, Chang P (1955) AICHE J 1: 264
22. Compton RG, Pilkington MBG, Stearn GM (1988) J Chem Soc Faraday Trans I 84: 2155
23. Booth J (1996) DPhil Thesis, Oxford University, Oxford, p 211
24. Verschuren K (1983) Handbook of environmental data on organic chemicals 2nd edn.